JOURNAL OF GEOPHYSICAL RESEARCH: SOLID EARTH, VOL. 118, 4586–4598, doi:10.1002/jgrb.50322, 2013

Recent estimates of Earth-atmosphere interaction torques and their use in studying polar motion variability

M. Schindelegger,[1] D. Salstein,[2] and J. Böhm[1]

Received 18 April 2013; revised 30 July 2013; accepted 1 August 2013; published 22 August 2013.

[1] The use of Earth-atmosphere interaction torques is a potential but generally less addressed alternative to the classical angular momentum approach for modeling variations in Earth rotation. We present an update on this subject for the purpose of explaining seasonal and intraseasonal polar motion variability based on the output of the most recent meteorological reanalysis systems of the ECMWF (European Centre for Medium-Range Weather Forecasts) and NASA's Global Modeling and Assimilation Office. The agreement of both models in terms of the three prime torque constituents is shown to be far superior to that of the conventionally deployed wind term of atmospheric angular momentum (AAM). A sufficiently good closure of the equatorial AAM budget equation within the ECMWF reanalysis provides additional endorsement for the use of atmospheric torques as excitation measures. When used as such, polar motion residuals after reduction of the AAM pressure term, as well as oceanic and hydrological excitation, are considerably better modeled by the torque-based quantities than by the standard wind term of AAM, in particular at intraseasonal periodicities. This finding is obtained by means of a newly proposed, hybrid excitation formalism, which derives the AAM counterparts of torque terms from inversion of the AAM budget equation in the frequency domain.

Citation: Schindelegger, M., D. Salstein, and J. Böhm (2013), Recent estimates of Earth-atmosphere interaction torques and their use in studying polar motion variability, *J. Geophys. Res. Solid Earth*, *118*, 4586–4598, doi:10.1002/jgrb.50322.

1. Introduction

[2] Considerable scientific interest has been conveyed in the irregular, geophysically driven fluctuations of the Earth rotation vector, in particular, its magnitude variations quantified as changes in length of day (LOD) and its movement with respect to a body-fixed reference frame reckoned as polar motion (or wobbles). Interpreting observational time series of these parameters in terms of the motion and mass redistributions in Earth's various subsystems is an illuminating but difficult task, relying on global numerical models of atmospheric and oceanic circulation as well as on the knowledge of terrestrial water storage and the interaction mechanisms between core and mantle.

[3] Over the last decade, advances of both geophysical observations and models as well as Earth rotation estimates from space geodetic techniques have allowed for a largely successful comparison of polar motion values and changes in LOD to modeled excitation signals, see *Gross* [2007] for a comprehensive overview. In short, nontidal perturbations of Earth's angular velocity at subdecadal periods are predominantly engendered by atmospheric dynamics [*Rosen and Salstein*, 1983], with oceanic and hydrological excitation providing small but nonnegligible contributions [*Chen et al.*, 2000]. The atmosphere's influence on polar motion from a few days to several years is less dominant than for the axial component and relates to large-scale pressure variations over northern midlatitude landmasses [*Nastula and Salstein*, 1999] and the corresponding changes in wind systems. The oceanic effect of mass-field variability and currents have been identified as the second main driving agent for seasonal and intraseasonal polar motion [*Ponte et al.*, 1998], while continental hydrology provides significant power in particular for the excitation of the annual wobble of amplitude of 90 mas (milliseconds of arc, or 2.7 m at the Earth's surface); see *Dobslaw et al.* [2010] for a recent, more detailed examination of those effects. Despite extensive modeling efforts, even a near-perfect closure of Earth's equatorial excitation budget has remained elusive on a wide range of time scales, including the annual period. These discrepancies are generally ascribed to still imperfectly represented dynamical processes as well as inconsistencies among the utilized circulation models [*Brzeziński et al.*, 2009; *Dobslaw et al.*, 2010].

[4] Two different but closely related approaches can be applied for investigating the impact of dynamical processes in any geophysical fluid on the rotation of the solid Earth. The first, more commonly used method derives from the

[1]Research Group Advanced Geodesy, Department of Geodesy and Geoinformation, Vienna University of Technology, Vienna, Austria.
[2]Atmospheric and Environmental Research, Lexington, Massachusetts, USA.

Corresponding author: M. Schindelegger, Research Group Advanced Geodesy, Department of Geodesy and Geoinformation, Vienna University of Technology, Gusshausstrasse 27-29, A-1040 Vienna, Austria. (michael.schindelegger@tuwien.ac.at)

2169-9313/13/10.1002/jgrb.50322

principle of angular momentum conservation in an Earth system isolated in space, encompassing both solid and fluid portions [*Munk and MacDonald*, 1960]. In such a system, the net change of angular momentum in the combination of the atmosphere, the oceans, land hydrology, and the core has to be balanced by a mirror image variation of angular momentum of the solid Earth, which in turn is detected by crust-bound geodetic stations as change in the rotation vector of the terrestrial reference frame. The elegance of such an angular momentum approach is augmented by computational advantages, as the involved global integrals are mostly robust quantities and can be evaluated based on the primary output of numerical circulation models [*de Viron et al.*, 2005a]. Early documentation of the geophysical origin of changes in LOD and polar motion via angular momentum estimates from globally gridded models of the atmosphere and the oceans is included in *Barnes et al.* [1983], *Rosen and Salstein* [1983], and *Ponte* [1997]. However, the specific processes that cause the solid Earth to alter its rotation can only be uncovered by a complementary method called *torque approach* [*Munk and Groves*, 1952]. This second approach conceives Earth's fluids as external layers to the mechanical system [*de Viron et al.*, 1999] and directly addresses the normal and tangential interaction forces across all subsystems' interfaces, taking into account the acting lever arm from the Earth's axis.

[5] Despite its potential and illustrative nature, the analysis of interaction torques at the Earth's surface in understanding the variability of Earth rotation has been less applied than the angular momentum approach. A mathematical framework is outlined in *Wahr* [1982] but it is generally less straightforward than the sophisticated schemes existing for excitation via angular momentum considerations [*Gross*, 2007; *Brzeziński*, 1994]. Few comprehensive torque studies exist for the case of polar motion [*Wahr*, 1983; *Bell*, 1994; *de Viron et al.*, 1999; *Fujita et al.*, 2002]; the majority of which point out computational and numerical difficulties in the evaluation of torque terms. Additional obstacles to the torque method consist in the need for fine spatial resolution of circulation models (particularly near sharp topographic features), the unavailability of specific surface fields, and poor observational constraints on the actual interaction forces [*de Viron et al.*, 2005a]. There are however good reasons to believe that these drawbacks have been considerably mitigated over the last decade for at least the atmospheric portion within the ensemble of numerical models for global geophysical fluids. Modern analysis and assimilation systems for the atmosphere rely on an increasing number of observations from a multitude of techniques, and are also subject to advances of the model physics and the inherent analysis modules, compare, e.g., *Dee et al.* [2011] with *Kalnay et al.* [1996]. Users and researchers can now access meteorological data with high spatial resolution (down to 16 km), while auxiliary surface variables such as instantaneous stresses have become available as well. These improvements provide the rationale for a renewed expectation of success in dealing with atmospheric torques in the context of Earth rotation.

[6] One key challenge when investigating both angular momentum and torques from a specific atmospheric model is to test the analytical equivalence between the two quantities. The evoked relationship is the angular momentum budget equation of a fluid layer overall, requiring that the time derivative of atmospheric angular momentum (AAM) equals the Earth-atmosphere interaction torque [*White*, 1949]. The validity of such a balance has been noted to be essential for the proper simulation of the general circulation as well as to avoid systematic errors in short-term forecasts that are utilized for LOD predictions in spacecraft navigation [*Huang et al.*, 1999]. Moreover, AAM and torque estimates can be cross-checked, and information on the quality of atmospheric models can be deduced since none of the existing analysis systems explicitly accounts for conservation of angular momentum. Extensive efforts have been devoted to the closure of the AAM budget in the axial direction, but dedicated simulations aside [*Lott et al.*, 2008], departures from an exact balance exist on various time scales [*Swinbank*, 1985; *Salstein and Rosen*, 1994; *de Viron and Dehant*, 2003]. The last study also represents the most recent assessment of the (intra)seasonal AAM balance in the equatorial direction and offers considerable room for improvement, too. As long as such a mismatch exists, one has to be critical of the application of torque series for quantifying the geophysical excitation of Earth rotation. If, by contrast, a sufficiently good closure of the AAM budget can be realized, it is justified to consider torques as complementary tools to the angular momentum method.

[7] This paper intends to present an update and extension of previous studies dealing with atmospheric torques in the context of Earth rotation, and specifically polar motion [*de Viron and Dehant*, 2003; *Feldstein*, 2008]. Motivated by the recent substantial advances of meteorological analysis systems, we examine novel equatorial torque estimates for (1) their agreement when computed from different atmospheric models, (2) their role in the AAM budget equation, and (3) their potential usability in studying polar motion variability on seasonal and intraseasonal time scales (i.e., periods from 4 to 400 days). The considerations are generally of numerical nature and based on the output of two of the currently most accurate atmospheric reanalysis systems: ERA-Interim of the ECMWF (European Centre for Medium-Range Weather Forecasts) [*Dee et al.*, 2011] and MERRA (Modern Era-Retrospective Analysis for Research and Applications) produced using the GEOS-5 global circulation model (Goddard Earth Observing System, Version 5) [*Rienecker et al.*, 2011]. Both angular momentum and torque data are derived in a consistent way from each reanalysis system and correspond with the time series of *Schindelegger et al.* [2013], who conducted a brief, basically time domain investigation on the atmospheric excitation of polar motion via the standard torque formalism of *Wahr* [1982]. The present study will greatly advance these tentative efforts, starting with a thorough term-by-term comparison of the same torque and angular momentum quantities through correlation and regression analyses (section 4). Verification of the equatorial AAM budget at intraseasonal and in particular seasonal frequencies (section 5) is the second key task of this study and another innovation compared to *Schindelegger et al.* [2013]. Finally, we explore the possibility of converting torques to AAM terms in the frequency domain and we assess the performance of these hybrid series with the evidence of polar motion observations, after accounting for additional oceanic and hydrological excitation signals (section 6).

2. Theoretical Considerations

2.1. Atmospheric Angular Momentum and Atmospheric Torques

[8] The angular momentum of the atmosphere (a) in the equatorial direction can be written as the complex quantity

$$\hat{H}^{(a)} = H_x^{(a)} + \mathrm{i}H_y^{(a)} = \Omega\Delta\,\hat{I}^{(a)} + \hat{h}^{(a)} = \hat{H}^{p} + \hat{H}^{w}, \qquad (1)$$

with Ω denoting Earth's mean angular velocity. The redistribution of air masses affects AAM both by small perturbations in the equatorial moments of inertia $\Delta\,\hat{I}^{(a)} = \Delta I_{xz}{}^{(a)} + \mathrm{i}\Delta I_{yz}{}^{(a)}$ as well as by changes in relative angular momentum $\hat{h}^{(a)} = h_x{}^{(a)} + \mathrm{i}h_y{}^{(a)}$ with respect to the body-fixed reference frame. Those two portions are conventionally called matter and motion terms or pressure and wind terms $\hat{H}^{p}$ and $\hat{H}^{w}$ in case of the atmosphere. The corresponding integrals utilize global surface pressure values and vertical profiles of wind velocities and can be found in numerous works, e.g., *Moritz and Müller* [1987]. In order to quantify atmosphere-induced variations of Earth rotation, pressure and wind terms are converted to *effective atmospheric angular momentum functions* [*Barnes et al.*, 1983]

$$\hat{\chi} = \hat{\chi}^{p} + \hat{\chi}^{w} = \frac{1.100}{(C-A')\Omega}\,\hat{H}^{p} + \frac{1.608}{(C-A')\Omega}\,\hat{H}^{w}, \qquad (2)$$

where A' and C are mean equatorial and axial moments of inertia of the entire Earth. The prefactors of pressure and wind terms account for the various responses of a realistic Earth model to rotational perturbations; see *Gross* [2007] for the exact derivation of equation (2). If available, oceanic angular momentum (OAM), as obtained from currents and ocean bottom pressure anomalies, can be simply superposed on the atmospheric quantities. Disregarding phenomena with diurnal or higher frequencies, the transfer function relating observed polar motion and geophysical excitation involves only the complex-valued, observed frequency of the Chandler Wobble $\hat{\sigma}_{cw}$ and reads [*Brzeziński*, 1994]

$$\hat{p} + \frac{\mathrm{i}}{\hat{\sigma}_{cw}}\dot{\hat{p}} = \hat{\chi}, \qquad (3)$$

with $\hat{p} = p_x - \mathrm{i}p_y$ being the reported position of the so-called Celestial Intermediate Pole (CIP) with respect to the terrestrial reference frame. Equatorial AAM as defined in equation (1) relates to the torque exerted by the solid Earth (s) on the atmosphere via the AAM budget equation in inertial space

$$\frac{\mathrm{d}\,\hat{H}^{(a)}}{\mathrm{d}t} = \hat{L}^{(s)\to(a)} = -\hat{L}^{(a)\to(s)} = \hat{L}^{e} + \hat{L}^{m} + \hat{L}^{f}, \qquad (4)$$

where the complex equatorial interaction torque $\hat{L}^{(s)\to(a)}$ is an integral measure of the local pressure, friction, and gravitational forces between the atmosphere and the solid Earth, see *Wahr* [1982] or *de Viron et al.* [1999] for a rigorous analytical treatment. Pressure and gravitational forces exerted by the flattening of the Earth on the atmosphere are the two dominant contributors to $\hat{L}^{(s)\to(a)}$ and usually noted as combined *ellipsoidal* or *equatorial bulge torque* $\hat{L}^{e}$. The *mountain torque* $\hat{L}^{m}$ quantifies remaining local effects associated with pressure gradients across topographic features, and also includes a minute contribution from the irregular Earth masses as represented by the local (nonbulge) geoid. A third but mostly minor contribution to the total interaction torque is due to the wind stress at the atmospheric boundary layer and is described by the *friction torque* $\hat{L}^{f}$. Sporadically, an additional constituent called *gravity wave drag torque* has been considered, which captures the local angular momentum exchange on spatial scales smaller than the grid size of the underlying atmospheric model. Given its smallness (< 0.5% of the total torque as computed from MERRA data) and the uncertainties of its parametrization [*de Viron and Dehant*, 2003], it will not be treated in the following.

[9] All equatorial torque terms can be computed as surface integrals, with their mathematical expression recently summarized in *Schindelegger et al.* [2013]

$$\hat{L}^{e} = \mathrm{i}\Omega\,\hat{H}^{p} = \frac{\mathrm{i}\Omega^{2}a^{4}}{g}\iint p_s \mathrm{e}^{\mathrm{i}\lambda}\cos\theta\sin^{2}\theta\,\mathrm{d}\theta\mathrm{d}\lambda, \qquad (5)$$

$$\hat{L}^{m} = -a^{2}\iint (a+h)\mathrm{e}^{\mathrm{i}\lambda}\left(\frac{\mathrm{d}p_s}{\mathrm{d}\lambda}\cos\theta - \mathrm{i}\frac{\mathrm{d}p_s}{\mathrm{d}\theta}\sin\theta\right)\mathrm{d}\theta\mathrm{d}\lambda, \qquad (6)$$

$$\hat{L}^{f} = -a^{3}\iint \mathrm{e}^{\mathrm{i}\lambda}\,(\mathrm{i}f_\theta - f_\lambda\cos\theta)\sin\theta\,\mathrm{d}\theta\mathrm{d}\lambda. \qquad (7)$$

Note that the sign of each component is consistent with that of the total torque acting *on* the atmosphere. The quantity a represents a mean Earth radius, g is the nominal gravity acceleration, $h = h(\theta,\lambda)$ denotes the topographic elevation above sea level [*Wahr*, 1982], and (θ,λ) are geographic colatitude and longitude. Differentiation of the surface pressure $p_s = p_s(\theta,\lambda)$ in both coordinate directions is essential for the mountain torque, while the friction torque depends on the colatitudinal and longitudinal wind stresses $f_\theta(\theta,\lambda)$ and $f_\lambda(\theta,\lambda)$. A central and helpful relationship for this study is indicated in equation (5), that is, $\hat{L}^{e}$, the torque associated with the equatorial bulge, is exactly proportional to the AAM pressure term. This equivalence has been derived by *Wahr* [1982] and is recapitulated from both a mathematical and physical point of view in *Marcus et al.* [2004].

2.2. The Angular Momentum Budget Equation

[10] Considering all introduced quantities and expressing the time derivative of pressure and wind terms in the nonrotating reference frame, the equatorial AAM budget in equation (4) becomes

$$\frac{\mathrm{d}\left(\hat{H}^{p} + \hat{H}^{w}\right)}{\mathrm{d}t} + \mathrm{i}\Omega\left(\hat{H}^{p} + \hat{H}^{w}\right) = \hat{L}^{e} + \hat{L}^{m} + \hat{L}^{f}. \qquad (8)$$

The left- and right-hand sides of the equation share the term $\hat{L}^{e} = \mathrm{i}\Omega\,\hat{H}^{p}$, which accounts for 60–90% of the full signal variability on (intra)seasonal time scales. Equation (8) will therefore naturally produce a well-closed budget [*de Viron et al.*, 1999] and a much more convincing test of the AAM balance within each atmospheric model can be constructed by removing the ellipsoidal effect and verifying the residual budget

$$\frac{\mathrm{d}\left(\hat{H}^{p} + \hat{H}^{w}\right)}{\mathrm{d}t} + \mathrm{i}\Omega\,\hat{H}^{w} = \hat{L}^{m} + \hat{L}^{f}. \qquad (9)$$

[11] We also seek to assess how AAM and torque terms perform with respect to each other when compared to real observations of polar motion. Initially, one might apply the AAM excitation scheme (equations (2) and (3)) on pressure and wind terms and a separate excitation scheme (e.g., equation (10) of *Fujita et al.* [2002] based on the torque

formalism of *Wahr* [1982]) for atmospheric torques. This approach however implies several problems that would lead to an a priori deterioration of the torque results. First, the analytical derivations of *Wahr* [1982] contain approximations such as $\mathrm{d}/\mathrm{d}t \ll \Omega$ that are valid at long periods but are insufficient at least for intraseasonal time scales. Second, observed polar motion of the CIP at discrete epochs needs to be converted to geodetic excitation in terms of the instantaneous rotation pole by two subsequent differentiations [*Schindelegger et al.*, 2013], producing possible numerical errors. And third, the oceanic excitation plays a major role in inducing polar motion variability and can be considered within the AAM method by simply superposing atmospheric and oceanic quantities. For the torque approach, the best procedure would be to derive the set of Earth-atmosphere-ocean interaction torques from a combined geophysical model, as done by *de Viron et al.* [2001]. That is clearly beyond the scope of this study, though, and one might consider introducing OAM values in Wahr's torque result, see e.g. *Fujita et al.* [2002]. Such an attempt however requires a clear picture of what is calculated and which effects (friction, pressure forcing, ellipticity) have been included in the ocean model and how they affect the atmospheric torques.

[12] The performance of AAM and torque terms is thus compared via an alternative approach. Equation (8) allows us to obtain $\hat{H}^{(a)} = \hat{H}$ from the pure knowledge of all Earth-atmosphere interaction torques $\hat{L}^{(s)\rightarrow(a)} = \hat{L}$ and additionally separate pressure and wind terms. (More precisely, only deviations in the global AAM value can be recovered from the torques acting on the atmosphere, although this fact does not restrict the validity of the subsequent considerations.) We achieve the conversion by rewriting the AAM budget in equation (8) as $\frac{\mathrm{d}\hat{H}}{\mathrm{d}t} + \mathrm{i}\Omega\ \hat{H} = \hat{L}$ and by noting its frequency domain equivalent

$$\mathrm{i}\sigma\ \hat{H}(\sigma)\mathrm{e}^{\mathrm{i}\sigma t} + \mathrm{i}\Omega\ \hat{H}(\sigma)\mathrm{e}^{\mathrm{i}\sigma t} = \hat{L}(\sigma)\mathrm{e}^{\mathrm{i}\sigma t}, \tag{10}$$

where $\sigma = 2\pi f$ and f signifies the two-sided frequency-vector in cycles per (solar) day (cpd) allocated to the Fourier coefficients $\hat{L}(\sigma)$ of the discrete complex signal $\hat{L}(t)$. Hence, the spectral components of the corresponding equatorial AAM are accessible by means of a simple transfer function, which is resonant at the retrograde diurnal frequency

$$\hat{H}(\sigma)\mathrm{e}^{\mathrm{i}\sigma t} = \frac{-\mathrm{i}}{\sigma + \Omega}\hat{L}(\sigma)\mathrm{e}^{\mathrm{i}\sigma t}. \tag{11}$$

Note that this result is also implicitly contained in the considerations of *Marcus et al.* [2004], who designate the resonance effect as *ill-conditioning* of the AAM budget equation in the retrograde diurnal band. Given a proper inverse transform to the time domain, the total AAM term $\hat{H} = \hat{H}(t)$ from equation (11) can be further divided into its wind and pressure portions, the latter equaling the ellipsoidal torque (equation (5)). As a result, the AAM wind term (called *equivalent wind term* in the following) is obtained from the torque-based total AAM via

$$\hat{H}^{w} = \hat{H} - \hat{H}^{p} = \hat{H} + \frac{\mathrm{i}}{\Omega}\hat{L}^{e}, \tag{12}$$

and does not have to be necessarily calculated from the vertical integration of wind velocities, which might be laborious and certainly requires considerable disk space. Instead, our frequency domain approach suggests that the variation of $\hat{H}^{w}$ with respect to its mean value is fully determined from the surface integral of local forces, in particular, if one neglects the small inadequacy (< 0.5%) of the thin layer approximation used in evaluating the equatorial bulge torque. This result is basically in agreement with equation (5.11) of *Wahr* [1982], albeit considerably more accurate at frequencies above the seasonal band. Further benefits of the proposed strategy are the computational convenience (no numerical integration or differentiation), the possibility to incorporate torque-derived quantities in the well-established AAM excitation scheme (equation (2)), and the avoidance of difficulties in the superposition of oceanic excitation (see paragraph below equation (9)). A certain drawback is that the physical interpretation of polar motion variations is somehow blurred, since (equivalent) AAM values are less insightful from a physical point of view. Moreover, the method is better suited for post-processing tasks than for real-time applications, as with each additional time step and torque value, the transfer function in spectral space (equation (11)) and its inverse transform to time domain (leading to equation (12)) have to be recomputed. Mean values of the x and y wind term components, usually reduced in any comparison to geodetic excitation, are not accessible either.

3. Data From Atmospheric Reanalyses and Their Preparation

[13] This study uses the gridded output of ERA-Interim and MERRA for the time span January 2007 to December 2010. ERA-Interim represents the most recent reanalysis effort of the ECMWF and extends from 1979 to near-real time. It has been specifically designed to address and improve on particular weaknesses of its predecessors, e.g., the long-term homogeneity or the precipitation and humidity cycles [*Dee et al.*, 2011]. The reanalysis results include consistently produced data on both the model surface and on specified vertical layers. We downloaded geopotential, specific humidity, temperature, eastward and northward wind speed grids on 25 pressure levels at 2° horizontal resolution, whereas surface pressure, eastward and northward surface stresses (f_λ and $-f_\theta$) were obtained as 2-D fields at 0.5° resolution. These surface data also include a static potential field (called *orography*), which, if converted to geometrical heights, is an instrumental variable for the evaluation of the mountain torque (equation (6)) and for the interpolation/extrapolation of meteorological data to the lower bound of vertical integration in the expression of the AAM wind term. All data were obtained and processed with an initial temporal resolution of 3 hours as provided by 12-hourly forecast arcs within the ERA-Interim variational analysis cycle. Such a dense sampling is not required for the purpose of this paper but was selected to prepare for subsequent work on diurnal and subdiurnal atmospheric torques.

[14] The second reanalysis model MERRA, conceived by NASA's GMAO (Global Modeling and Assimilation Office) as a climate context to a host of satellite missions, was approached in similar manner. We downloaded 3-hourly, 3-D data on the same 25 isobaric levels as for ERA-Interim at 1.25° resolution under product name *3D assimilated state on pressure* from the MERRA data holdings at http://disc.sci.gsfc.nasa.gov/mdisc/data-holdings. This stream also provides access to surface pressure and the model's intrinsic

orography. Hourly eastward and northward stresses are available at the native grid resolution of $1/2° \times 2/3°$ from the same website under product name *IAU 2D surface-turbulent flux diagnostics*. Note that those stresses are time-averaged values centered across the hourly intervals, while ERA-Interim's stresses are instantaneous fields. The data sources for each reanalysis were selected with great care in order to minimize inconsistencies between the different meteorological grids required for the angular momentum and torque approaches [*de Viron et al.*, 2005b], thus ensuring good preconditions for an AAM budget validation. This is particularly true for all ERA-Interim quantities, as they are homogeneously deduced from forecast fields.

[15] Auxiliary geophysical fluids data in this study include (effective) angular momentum functions for both the global ocean and the continental hydrology as presented in *Dobslaw et al.* [2010]. The respective models are the Ocean Model for Circulation and Tides (OMCT) [*Thomas et al.*, 2001] and the Land Surface Discharge Model (LSDM) [*Dill*, 2009], which are both driven by momentum and energy fluxes from ERA-Interim atmospheric fields under consideration of global mass conservation. It is thus justified to combine AAM or torque data from ERA-Interim with the given oceanic and hydrological excitation series as done in section 6. Small inconsistencies may be elicited since OMCT and LSDM are forced with 6-hourly analyzed states instead of short-term forecasts, although the negative effects of this mismatch are certainly larger for high-frequency phenomena than on intraseasonal or longer time scales. The inclusion of hydrological angular momentum can be debated, given its known uncertainties (H. Dobslaw, personal communication, 2013). Yet, we retain the associated excitation functions as part of a fully consistent, mass-conserving dynamical system, cf. *Dobslaw et al.* [2010]. Core effects, which are even less well known but usually cited as possible sources for decadal variations of the observed polar motion [*Greiner-Mai and Barthelmes*, 2001] are neglected in the subsequent analysis of seasonal and intraseasonal signals.

[16] Discretization of the AAM formulae and the torque expressions (equations (5)–(7)) allows computing the equatorial AAM pressure and wind terms, as well as ellipsoidal, mountain, and friction torques at the temporal resolution of the described meteorological data. For the determination of pressure gradients, we utilized a second-order centered finite difference scheme investigated also by *Huang and Weickmann* [2008]. Although slightly more accurate schemes exist from a numerical point of view, we note that the surface pressure fields in this work are given with higher resolution than those of *Huang and Weickmann* [2008] and that a possibly introduced bias is eliminated in any case by detrending all time series.

[17] Furthermore, one has to ponder on the role of the inverse barometric (IB) response of the oceans in the various quantities. For Earth rotation studies at periods ≥ 5 days, an IB-corrected AAM pressure term is conventionally deduced as the average atmospheric pressure over the oceans. Hence, if IB AAM functions and oceanic excitation are superposed, the relevant oceanic mass term needs to represent only the deviation from an ideal IB behavior. This is the case for the available OMCT results, as ocean bottom pressure anomalies (measuring the mass of the water column and the air column aloft) have been reduced by the mean atmospheric (IB) pressure, see *Dobslaw et al.* [2010]. By implication, we need to correct the atmospheric quantities accordingly, i.e., impose the IB approximation on both the AAM pressure term or its torque equivalent, the ellipsoidal torque [*Marcus et al.*, 2010]. Non-IB series of pressure terms and ellipsoidal torques were also produced in order to assess the purely atmospheric angular momentum budget and derive the equivalent wind term. All time series (except the slowly varying hydrological excitation) underwent low-pass filtering (fifth-order Butterworth with cutoff frequency at 0.5 cpd) and resampling at daily intervals. This preprocessing ensures a good fit to the daily C04-solution of the International Earth Rotation and Reference Systems Service, which provides the observed polar motion for 2007–2010.

4. Analysis of AAM and Torque Terms

[18] As a preparatory analysis step, we investigated the (non-IB) ellipsoidal, mountain, and friction torque contributions to the total Earth-atmosphere interaction torque at various frequencies based on the discrete Fourier transforms of the complex-valued signals $\hat{L}^e$, $\hat{L}^m$, and $\hat{L}^f$ from ERA-Interim. Each of the three two-sided spectra was sampled at frequency steps of 0.5 cycles per year (cpy), with spectral content at a bandwidth of ± 2 cpy around the central sampling frequency being retained but down-weighted by means of a standard Hanning window. We then expressed the average modulus from each of those bins for ellipsoidal, mountain, and friction torques as fraction of their sum $\left|\hat{L}^e(\sigma)\right| + \left|\hat{L}^m(\sigma)\right| + \left|\hat{L}^f(\sigma)\right|$ (as opposed to the modulus of the phasor sum, which might be smaller than its constituents due to cancelation effects). While this procedure, including the choice of spectral parameters, is not unchallengeable, it serves its purpose to give a smooth picture of the respective torque amplitudes at prograde and retrograde frequencies (Figure 1). As anticipated, the bulge effect dominates the other two constituents on all time scales, with magnitude ratios of 95% at the annual frequency and ~80% for semi-annual and terannual, as well as intraseasonal periodicities down to 10 days, cf. also the (IB) amplitude estimates of *Gross et al.* [2003]. The significance of the mountain torque increases with higher frequencies and becomes comparable to the ellipsoidal torque near the diurnal band, whereas the contribution of $\hat{L}^f$ to the cumulative modulus never exceeds 5% at periods longer than 4 days. This size of effect is non-negligible for the present study but also indicates that the magnitude relationship of mountain and ellipsoidal torques is very similar to that of the AAM wind and pressure term pair, i.e., $\hat{L}^e = \mathrm{i}\Omega\,\hat{H}^p$ and $\hat{L}^m \approx \mathrm{i}\Omega\,\hat{H}^w$ as seen from equation (9) for $\mathrm{d}/\mathrm{d}t \ll \Omega$.

4.1. Pressure and Wind Terms

[19] The comparison of the same AAM quantities from the two atmospheric models was realized on the basis of correlation and regression analyses at spectral intervals of $\Delta\sigma = 0.5$ cpy in the manner of *de Viron et al.* [1999]. We designed a second-order infinite impulse response peak filter [*Proakis and Manolakis*, 1996] with bandwidth ± 2 cpy to extract the residual signals from the pressure term (or wind term) time series of ERA-Interim and MERRA. From

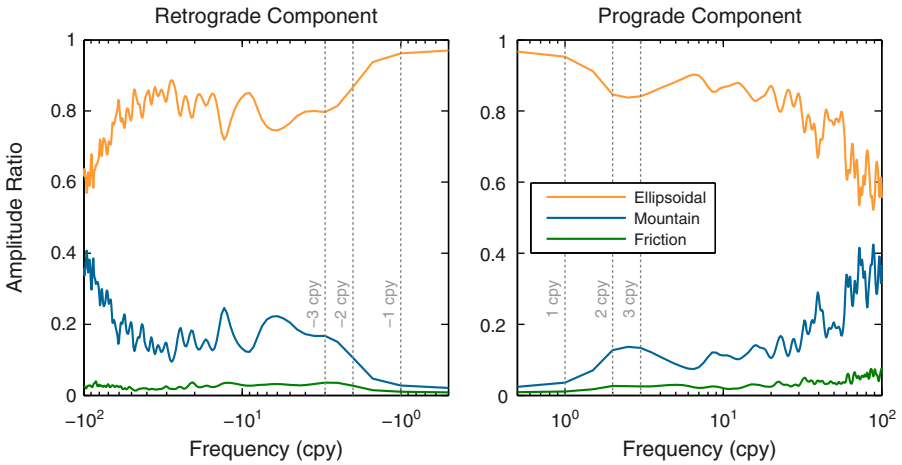

Figure 1. Frequency-dependent ratios of the ellipsoidal torque (orange curve), mountain torque (blue curve), and friction torque (green curve) amplitudes from ERA-Interim with respect to the sum of amplitudes from all three constituents.

the time domain comparison of those residuals, their linear dependency (correlation coefficient) and scale factor (regression coefficient, with ERA-Interim regressed against MERRA) were deduced. Both values should ideally be 1. This requirement is almost perfectly met by the x and y components of the AAM pressure term (Figure 2a), especially for frequencies lower than 60 cpy. Marginally less variable regression coefficients are evident for H^p_y, which is mainly sensitive to large-scale pressure variations over the continents and is thus well supported by the huge amount of barometric and other land-based observations common to both ERA-Interim and MERRA.

[20] Figure 2b reveals much larger discrepancies in the comparison of relative angular momentum from the two reanalysis data sets. Both x and y cross-spectra show irregular peaks and notches around a mean correlation and regression level of about 0.9. Scale deviations in the representation of seasonal wind oscillations are particularly conspicuous for the y component. These substantial differences in the wind term in contrast to the excellent match seen for $\hat{H}^p$ are in part expected in light of earlier comparisons of the same kind, e.g., *Eubanks et al.* [1988]. In a detailed investigation of wind field differences in the context of Earth rotation, *Masaki* [2008] found that most of the

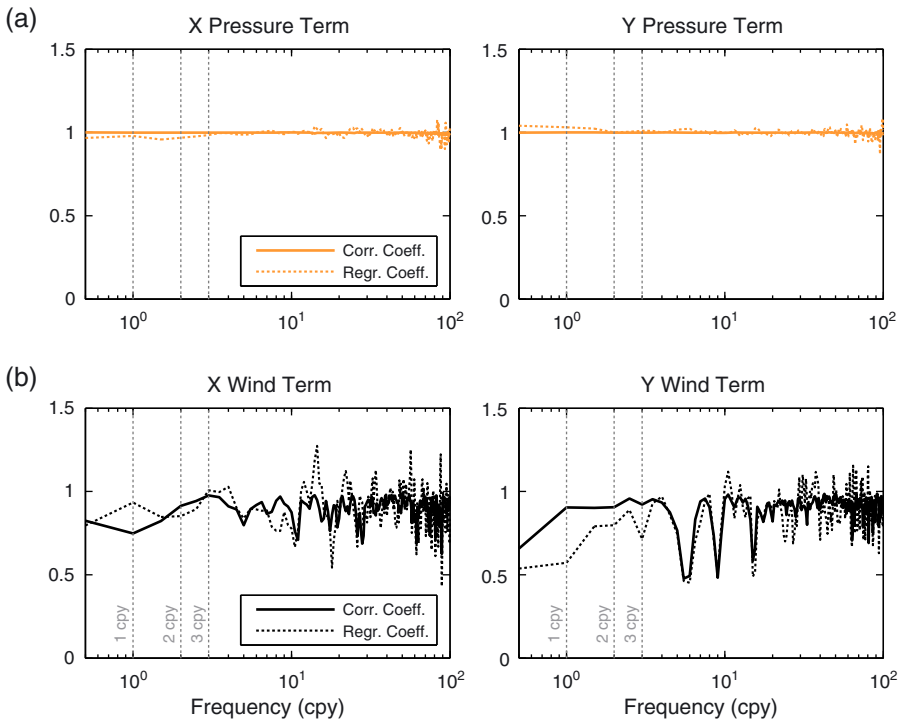

Figure 2. Frequency-dependent correlation coefficients (solid curves) and regression coefficients (dashed curves) for (a) the pressure term and (b) the wind term of ERA-Interim and MERRA.

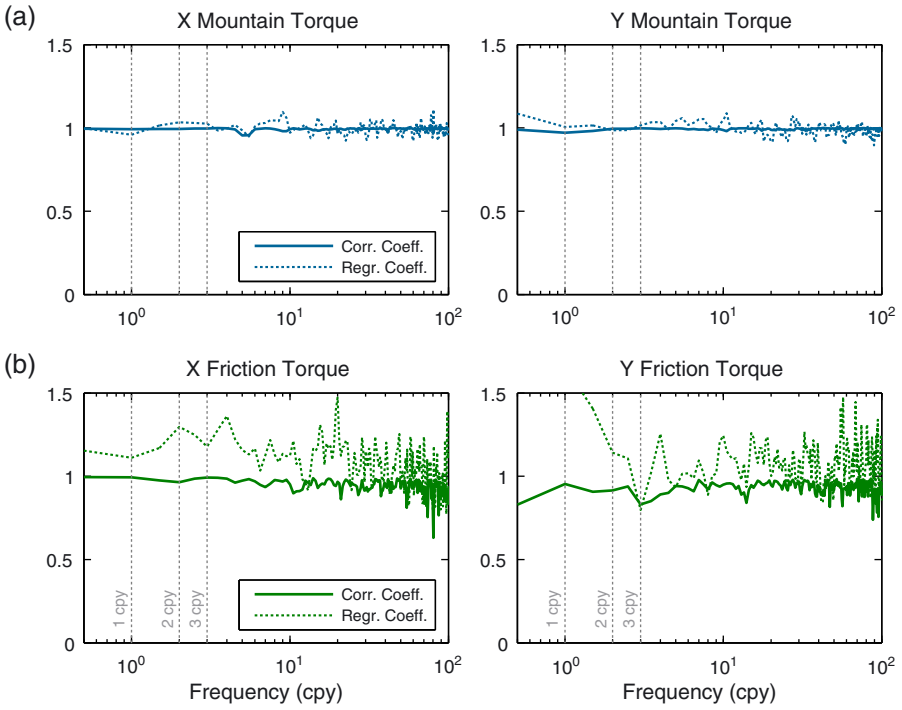

Figure 3. Frequency-dependent correlation coefficients (solid curves) and regression coefficients (dashed curves) for (a) the mountain torque and (b) the friction torque of ERA-Interim and MERRA.

differences of equatorial AAM functions originate from the uncertainty of northward wind speeds in the upper troposphere over southern midlatitudes and tropical regions. This result, presumably reflected in Figure 2b, is of direct concern for excitation estimates of polar motion as the wind term accounts for 10–50% of the atmosphere-driven intraseasonal polar motion and is also nonnegligible at seasonal frequencies, see *Gross et al.* [2003]. Hence, information on the reliability of both ERA-Interim and MERRA wind terms is precious and will partially be provided by evaluating the residual AAM budget equation in section 5.

4.2. Mountain and Friction Torques

[21] With the cross-spectra of the ellipsoidal torque being equivalent to that of the AAM pressure term (only reversed roles of x and y), we directly address the analysis of the mountain torque in Figure 3a. The displayed correlation and regression series appear to be only marginally worse than those of the ellipsoidal torque. This is a remarkable result given that $\hat{L}^e$ arises from the surface integration of global-scale pressure patterns, whereas $\hat{L}^m$ reacts to local, high-terrain pressure gradients, which are believed to be less well known [*de Viron et al.*, 2005a]. Another positive finding is that the different horizontal resolutions of the ERA-Interim and MERRA surface pressure grids (0.5° and 1.25°, respectively) do not cause any significant differences in the globally integrated mountain torques, even though $\hat{L}^m$ is, in principle, sensitive to the small-scale variability of pressure and topography [*de Viron and Dehant*, 2003]. If the latter study is taken as a benchmark for the numerical agreement achievable for torque quantities from meteorological reanalyses a decade ago, we get one of the key results of the present paper, that is, the coherence between equatorial mountain torques from different atmospheric models has substantially improved from a level of 0.8 (or less) to nearly 0.99 at seasonal and intraseasonal periodicities (coherence plot not shown, but Figure 3a gives an indication). It has to be acknowledged that *de Viron and Dehant* [2003] probed much longer reanalyis runs, spanning roughly three decades (1968–1999), which is in stark contrast to the 4 year test data set examined here. On a second note, we again stress the relative contribution of the mountain torque to the total atmospheric torque being very similar to that of the wind term to the cumulative AAM. Both $\hat{L}^m$ and $\hat{H}^w$ thus play about the same role in their respective approaches. However, the numerical results (cf. Figures 2b and 3a) echo a much better convergence of the reanalysis models in terms of mountain torque values, testifying that $\hat{L}^m$ represents a stable excitation measure from different data sets. Whether the obtained mountain torque series are realistic or not can only be judged within a comparison to geodetic excitation of polar motion.

[22] Further discussion is inspired by the cross-spectra of the friction torque (Figure 3b), which displays a high level of correlation ($\sim$0.93) throughout the investigated frequency bands. The regression analysis indicates that one model (ERA-Interim) by tendency produces larger friction torque amplitudes than the second model (MERRA) by about 10–50% on different time scales, albeit the underlying grid resolution for both flux data sets is almost identical (section 3). Overall, the agreement between the different estimates for $\hat{L}^f$ is very high and can be compared to that obtained by *de Viron and Dehant* [2003] for previous reanalyses of the ECMWF and NCEP (National Center for Environmental Prediction). Interestingly, the coherence of equatorial friction torques between the predecessors of

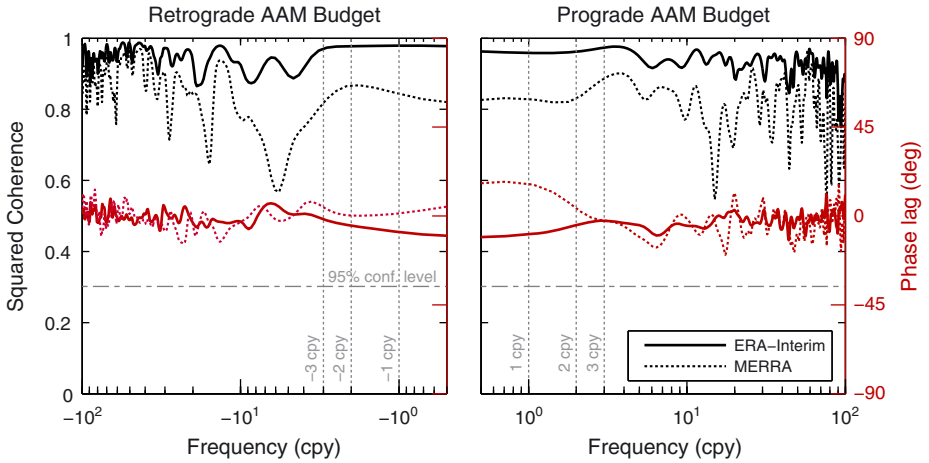

Figure 4. Frequency-dependent magnitude-squared coherence and phase lag values of the sum of local torques and the residual AAM time derivative for ERA-Interim (solid curves) and MERRA (dashed curves).

ERA-Interim and GEOS-5 was also investigated by *de Viron and Dehant* [2003] but found to be very low at intraseasonal periods. Figure 3b represents a major improvement to that effect, even though one has to consider that the underlying surface stresses are not observed directly but largely controlled by the turbulence parametrization scheme and the physical model equations [*Dee et al.*, 2011]. Both ERA-Interim and MERRA presumably show strong similarities in this respect.

[23] Finally, we note a clear deterioration of correlation and regression values at seasonal periodicities for the *y* component of the friction torque in analogy to the *y* component of the global wind term in Figure 2b. A plausible explanation for this observation arises from the fact that both terms $\left(L_y^f \text{ and } H_y^w\right)$ share the same sensitivity patterns for northward and eastward vector components, i.e., wind velocities and surface stress values, respectively. It is likely that uncertainties in the wind profiles have a bearing on the wind stress representation in each of the atmospheric models.

5. Analysis of the Angular Momentum Balance

[24] Due to the dominance of the (non-IB) bulge effect in both AAM and the total torque, equation (8) is virtually perfectly closed over the entire frequency range and provides no particular insight into the quality of the reanalysis data sets. By contrast, the residual AAM budget in equation (9) allows us to cross-check the remaining players $\hat{H}^w, \hat{L}^m$, and $\hat{L}^f$ and assess the balance between those terms within ERA-Interim and MERRA. We opted for an analysis of coherence and phase lag values at prograde and retrograde frequencies based on the built-in MATLAB functions *mscohere* (magnitude-squared coherence) and *cpsd* (cross power spectral density) with $n_f = 2^{10}$ frequency samples and a Hamming window function of length $n_f/4$. This configuration produces smooth spectra with a level of detail similar to a windowless implementation. Considering that the default lag window overlap of 50% doubles the smoothing factor of the spectral estimator, the 95% confidence level of the squared coherence amounts to 0.30, cf. equation (9.2.23) of *Jenkins and Watts* [1968].

[25] The results are presented in Figure 4 and unambiguously reveal ERA-Interim as the "better" of the two reanalysis models with regard to the residual AAM budget. Phase differences between the AAM time derivative and the sum of mountain + friction torques from ERA-Interim never exceed ±10°, while their coherence is usually above 0.9 up to the highest frequencies considered. Such a good closure constitutes another step forward from similar but less encouraging verifications of *de Viron and Dehant* [2003]. Yet, the AAM budget is only partly balanced within MERRA, with distinct drops in coherence found at the same frequencies (near –6 cpy and ±15 cpy) as the notches of the *y* AAM wind component in Figure 2b. We perceive this finding as an indication of the low reliability of the MERRA wind term in contrast to that of ERA-Interim. Caution should be therefore exercised if the output of MERRA is used to account for the atmospheric excitation of polar motion.

[26] In order to underpin the fine balance of the residual AAM budget within ERA-Interim in the seasonal band, Figure 5 assembles the contributing quantities in the complex plane expressed as phasors in units of hadleys (1 Hd = 10^{18} kg m^2). At such long periods, the AAM contribution on the left-hand side of equation (9) is governed by the term $i\Omega\ \hat{H}^w$ to about 95%. The cumulative mountain and friction torque is in excellent agreement with this quantity for all seasonal periodicities with minor exceptions in the retrograde semiannual and terannual bands. As expected from Figure 4, the analogous phasor plots for MERRA (not depicted) are less convincing, with the largest differences to the ERA-Interim budget visible for the seasonal components of the AAM wind term. Nonetheless, friction and, in particular, mountain torque estimates closely resemble those shown in Figure 5.

6. Comparison With Geodetic Excitation

[27] Motivated by the remarkable angular momentum balance within the ECMWF reanalysis, we compared AAM and torque time series from ERA-Interim with observed polar motion. Both types of excitation measures were deployed in the same transfer functions (equations (2) and (3)) so as to

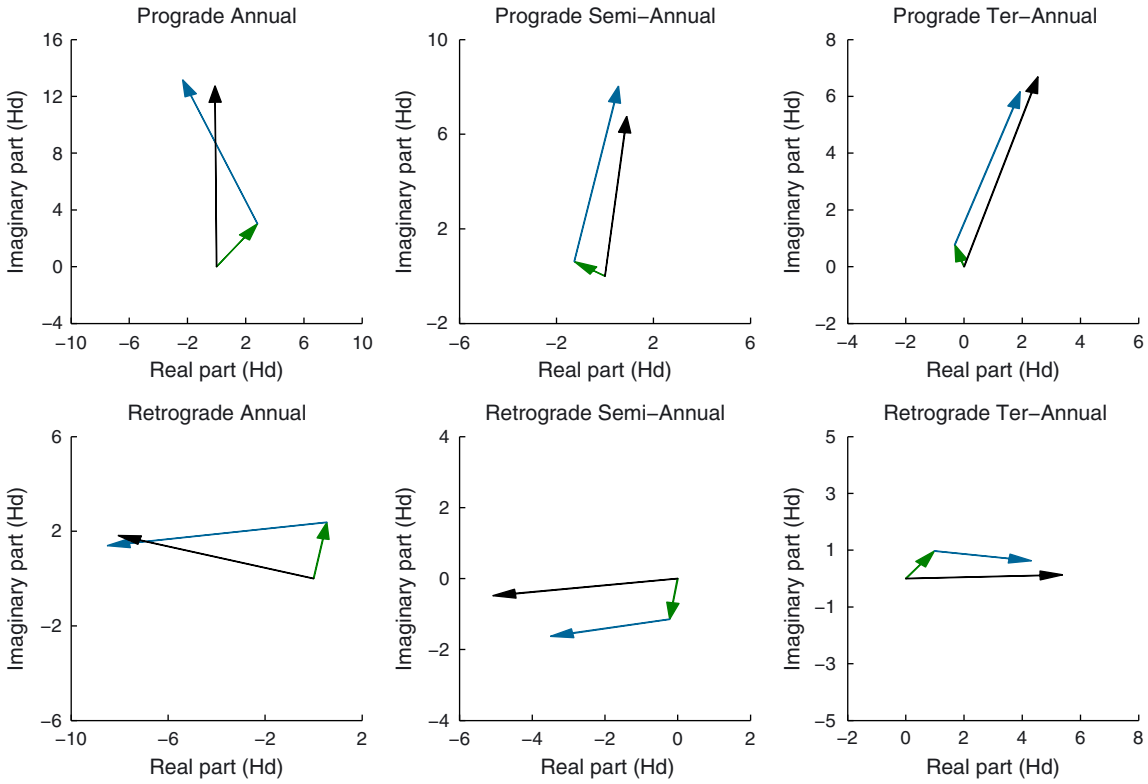

Figure 5. Phasor diagram for the residual AAM budget equation at prograde and retrograde seasonal frequencies, involving friction torque (green arrows), mountain torque (blue arrows) and the AAM time derivative (black arrows) from ERA-Interim in units of hadleys. The individual phasors were extracted as complex coefficients from the discrete Fourier transfrom of each series without a particular phase convention.

meet our requirement of even-handed treatment for AAM and torque terms, see section 2.2. Whereas the main contributor to equation (2), $\hat{H}^p$, is common to both approaches, and also $\hat{H}^w$ is readily available in case of the angular momentum approach, the equivalent wind term as determined from the total atmospheric torque needs to be computed from the frequency domain inversion of the AAM budget equation as given by equation (11). This task involves the discrete, two-sided Fourier transform (DFT) of $\hat{L}(t)$ and its associated frequency-vector

$$\sigma = \frac{2\pi}{n_f \Delta t}\left[-n_f/2, -n_f/2+1, \ldots, n_f/2-1\right], \qquad (13)$$

where Δt is the equidistant sampling rate (1 day). The DFT size, n_f, was fixed to the length of the analyzed time series, guaranteeing the desired daily time domain sampling after inverse DFT without any noticeable numerical degradation. Real and imaginary parts (or x and y components) of the equivalent wind term, eventually deduced from equation (12) in the time domain, are displayed in Figure6 together with the original AAM wind term from vertical integration. The apparently close match of the two series confirms that the suggested procedure gives very good results, considerably superior to that of Wahr's approximation $\hat{H}^w \approx -\mathrm{i}\left(\hat{L}^m + \hat{L}^f\right)/\Omega$, which was also tested. Small differences can be anticipated from Figure 6 for the high-frequency variation of the wind term.

[28] While all foregoing analyses utilized non-IB quantities, the actual comparison to geodetic polar motion requires the IB version of the AAM pressure term to ensure consistency with the IB-corrected ocean bottom pressure anomalies from OMCT. Accepting this formalism, effective angular momentum functions were obtained according to equation (2) for the atmosphere (a) (one set for the original wind term, one for its torque equivalent), the global ocean (o), and the continental hydrology (h) from the ERA-Interim-forced OMCT and LSDM models, respectively. Their superposition should balance the geodetic excitation function deduced from equation (3), or equivalently,

$$\hat{p} + \frac{\mathrm{i}}{\hat{\sigma}_{cw}}\dot{\hat{p}} - \left(\hat{\chi}^{(o),p} + \hat{\chi}^{(o),w}\right) - \left(\hat{\chi}^{(h),p} + \hat{\chi}^{(h),w}\right) - \hat{\chi}^{(a),p} \approx \hat{\chi}^{(a),w}, \qquad (14)$$

where $\hat{p}$ was taken from the C04-solution for 2007–2010 and the numerical values for $\hat{\sigma}_{cw}$ correspond to that of *Schindelegger et al.* [2011]. Equation (14) allows us to single out the respective performances of the standard wind term and the equivalent wind term with the evidence of polar motion residuals. Statistical measures of this comparison are specified in Table 1 and include the correlation coefficient ρ between the left- and right-hand sides of equation (14) as well as the root mean square (RMS) values of the total residuals $\hat{p} + \dot{\hat{p}}\mathrm{i}/\hat{\sigma}_{cw} - \hat{\chi}^{(a)} - \hat{\chi}^{(o)} - \hat{\chi}^{(h)}$ in the x and y directions.

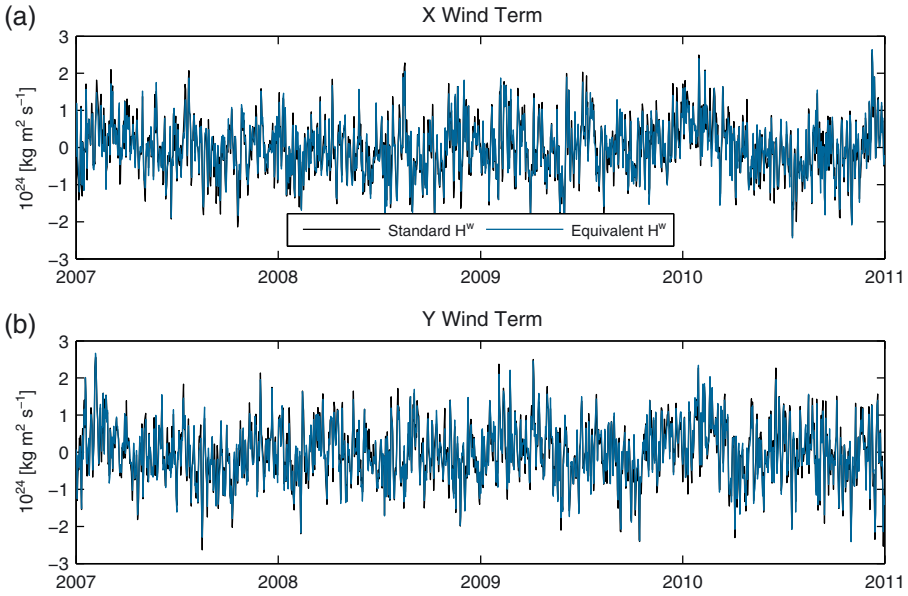

Figure 6. ERA-Interim wind term in (a) x and (b) y direction both from standard calculation (black curves) and torque quantities (blue curves) via inversion of the AAM budget equation. Small trends were removed from the standard wind term series.

[29] By including the atmospheric wind term in the excitation relationship, the variability of polar motion residuals as expressed by the RMS values in mas is generally reduced from a level of 19.6 mas to 16.1 mas in x and from 25.1 mas to 21.6 mas in the y direction. At a first glance, the y component of geodetic excitation, which is known for its larger overall spectral power (cf. *Schindelegger et al.* [2013]), does not react to whether the original wind term or its torque equivalent is deployed, as the correlation coefficient is 0.51 for both variants. However, truly encouraging results are evident for the x component, which, partly due to its lower level of variability, is capable of revealing an increased correlation of 0.62 for the equivalent wind term compared to 0.58 for the standard case. The associated RMS reduction (0.7 mas) is significant at the $\alpha = 0.05$ level (95% confidence interval), as judged from the F (Fischer) test of the quotient of squared RMS differences [*Bosch*, 1996]. It is therefore justified to assume that the torque-based wind term, which mainly arises from the surface pressure gradients over land, can reduce the vulnerability of the AAM wind term to uncertain vertical wind profiles over the tropical oceans [*Masaki*, 2008]. The argument of deficient wind data was already presented in section 4. It might especially hold for the x component of the AAM wind term, of which the weighting pattern $[\sin\lambda \sin\theta]$ for northward wind speeds peaks right over the problematic regions noted by *Masaki* [2008] (east Pacific and Indian Ocean). The finding that the statistical measures are not improved by the torque-based quantities in y is partly refuted in Table 2 by a completely analogous comparison to Table 1 for intraseasonal periodicities only. The separation of frequency bands was accomplished by means of a fifth-order Butterworth high pass (cutoff at 3 cpy) and reveals ρ = 0.52/RMS = 19.9 mas instead of ρ = 0.50/RMS = 20.2 mas for the standard wind term in y direction. However, the null hypotheses of no ρ/RMS improvement in Table 2 can only be rejected at markedly low-significance levels ($\alpha = 0.46$ for the correlation coefficient, $\alpha = 0.29$ for the RMS differences). These slight corrections are masked in Table 1 by the inclusion of seasonal frequencies, what in turn demonstrates the good quality of the seasonal ERA-Interim wind term and (or) remaining uncertainties in the local torques. We also repeated the above analysis excluding the hydrological excitation functions in equation (14) and arrived at basically the same numerical results.

[30] Table 1 is also extended by the analogous values from the second reanalysis, MERRA. Although the superposition of AAM terms from this data set evokes strong inconsistencies with the atmospheric forcing of the ocean and land hydrology model, the benefit of using torque-based wind terms is evident from a 7% increase of correlation and

Table 1. Statistical Measures for the Comparison of Geodetic Excitation to AAM Functions From ERA-Interim and MERRA: Correlation Coefficient ρ Between Standard as Well as Equivalent Wind Terms and Polar Motion Residuals (Atmospheric Pressure Term, Oceanic and Hydrological Excitation Subtracted); Corresponding RMS Values in x and y Direction for the Total Polar Motion Residuals (as Defined in the Text)[a]

		ρ		RMS (mas)	
		x	y	x	y
ERA-Interim	Standard wind term	0.58	0.51	16.1	21.6
	Equivalent wind term	0.62	0.51	15.4	21.6
Significance level α of F test		9%	-	5%	-
MERRA	Standard wind term	0.54	0.42	16.5	23.1
	Equivalent wind term	0.61	0.49	15.4	21.9
Significance level α of F test		1%	2%	1%	2%

[a]The significance level α in refuting the null hypothesis of no increase in correlation has been computed from the F transformation of both ρ values (standard wind term, equivalent wind term) following *Bosch* [1996]. A simple F test on the quotient of squared RMS differences yielded the significance level of the RMS reduction.

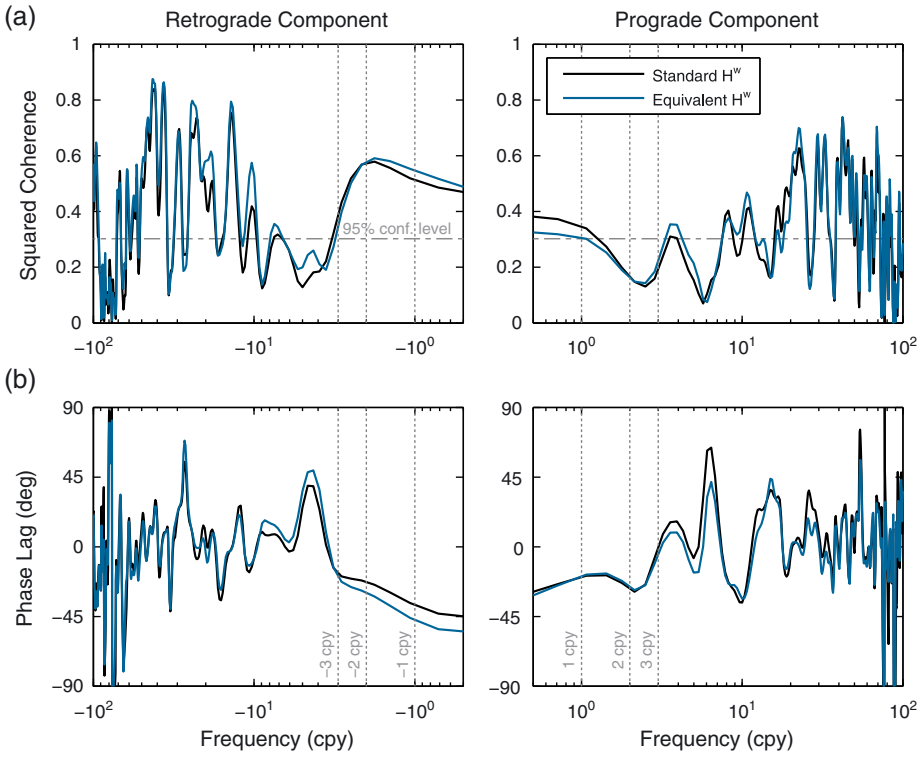

Figure 7. Frequency-dependent (a) magnitude-squared coherence and (b) phase lag values of wind term and geodetic excitation after reduction of the atmospheric pressure term, as well as oceanic and hydrological excitation. Results for both the standard wind term (black curves) and the equivalent wind term (blue curves) are depicted. The 95% confidence level of the squared coherence has been constructed following *Jenkins and Watts* [1968].

from RMS values reduced by 1.1–1.2 mas with respect to MERRA's standard wind term. Together with Figure 4, this result illustrates the lack of reliability of $\hat{H}^w$ as obtained from vertical integration of MERRA wind velocities.

[31] As a final comparison, we derived coherence and phase lag plots for the left- and right-hand sides of equation (14) with the same settings as introduced in section 5. Figure 7a displays the magnitude-squared coherence between polar motion residuals and the wind terms from the two investigated approaches (only ERA-Interim). The best match between $\hat{H}^w$ and the residual geodetic excitation is generally found between 20 and 50 cpy for both prograde and retrograde frequencies, where the pressure term contribution substantially diminishes (Figure 1). In accordance with the statistical results in Tables 1 and 2, the equivalent wind term yields marginally higher coherence values at nearly all periodicities, in particular, those below the seasonal bands. For semiannual and annual wobbles, the standard wind term again appears to perform somewhat better; see also the slightly smaller phase discrepancies in Figure 7b. Apart from these findings, the imperfect phase lag values in Figure 7 and low-coherence estimates (partly below the 95% confidence limit) are also a testament to the still existing leakage in the excitation budget of geodetic polar motion. Further reduction of the gaps at seasonal and subseasonal frequencies certainly awaits the improvement of oceanic (and hydrological) circulation models [*Brzeziński et al.*, 2009].

Table 2. As Table 1 but Only for ERA-Interim and Intraseasonal Periodicities

		ρ		RMS (mas)	
		x	y	x	y
ERA-Interim	Standard wind term	0.59	0.50	14.4	20.2
	Equivalent wind term	0.63	0.52	13.8	19.9
Significance level α of F test		8%	46%	6%	29%

7. Conclusion and Outlook

[32] Two novel, 4-year records of equatorial torques acting on the atmosphere have been computed, cross-checked, and validated against geodetic observations of polar motion. The three major findings from these numerical considerations are as follows: (1) the agreement between the chosen reanalysis data sets (ERA-Interim and MERRA) in terms of local torques has significantly improved from similar comparisons of previous studies and clearly exceeds the match achievable for the more routinely used AAM wind term; (2) torque and angular momentum quantities from ERA-Interim provide an impeccable closure of the residual AAM budget equation on seasonal and intraseasonal time scales, after removal of the dominant forcing associated with Earth's equatorial bulge; such a balance is a strong indication of the reliability of mountain and friction torques for further use in the context of Earth rotation; (3) when converted to AAM terms and inserted into a sophisticated

excitation formalism, torque quantities perform marginally better in explaining intraseasonal polar motion variability than their AAM counterparts. Provided a careful selection of the underlying meteorological data, we thus dare to believe that for restricted periodicities, the margin between angular momentum and torque approaches for the atmosphere has become much finer than previously noted.

[33] Even though our results are unambiguous, they are also tentative to some extent. First and foremost, a third atmospheric reanalysis data set should be analyzed in an analogous way in order to substantiate the deduced results for ERA-Interim and MERRA. These independent torque and angular momentum estimates can be in principle obtained from the current Climate Forecast System Reanalysis (CFSR) [*Saha et al.*, 2010] of NCEP. On another note, it would be desirable to extend the time frame of our study to the full reanalysis period (commencing 1979), thereby enabling AAM budget considerations over three decades of substantial advances in atmospheric models/assimilation systems, and also a thorough comparison to the findings of *de Viron and Dehant* [2003]. Validation against geodetic excitation, both on a year-to-year basis and as a long-term mean, would help to ascertain our results from the present 4-year test data set.

[34] A more comprehensive assessment is also due for the anomalous wind term of MERRA. We suggest a study of regional discrepancies in wind speeds on specific vertical layers, including analysis fields of ERA-Interim and NCEP's CFSR. This approach can provide a hindsight on the possible influence of radio occultation measurements [*Kursinski et al.*, 1997], which have not been considered in MERRA prior to 2011 but provide the third most important data volume in ERA-Interim since 2007 (cf. *Dee et al.* [2011]) and are also assimilated in CFSR (cf. *Saha et al.* [2010]). Radio occultation retrievals are high-resolution soundings at altitudes from 40 km to near-ground layers. They thus directly support the representation of atmospheric dynamics in regions of high density, which are of utmost importance for AAM wind signals.

[35] Further extensions of this work include the axial component of Earth rotation as well as analogous investigations at diurnal and subdiurnal time scales [*de Viron et al.*, 2005b], for which the respective contributions of equatorial torque terms is somewhat different to that at lower frequencies. Given the resonance condition of the AAM budget inversion at retrograde diurnal frequencies, the suggested hybrid excitation formalism has to be reassessed and perhaps refined.

[36] The ultimate goal for the torque method would consist in an application on a realistic, coupled atmosphere-ocean model in order to compute the total atmospheric + oceanic torque on the solid Earth. While such an approach can be enlightening in terms of the interaction processes between all subsystems, it is also a complex problem putting high requirements on the oceanic portion of the model, e.g., a precise knowledge of local water column heights due to the friction drag at the sea surface [*de Viron et al.*, 2005a]. On top of that, the excitation formalism for torque quantities suggested by *Wahr* [1982] is only of approximative nature at subseasonal periodicities and needs to be advanced in its own right. The impact of ocean dynamics on Earth rotation should thus be preferably estimated via the classical angular momentum approach. Nevertheless, it will be an interesting challenge to exploit future model advances to understand dynamic interactions between Earth system components in the torque framework.

[37] **Acknowledgments.** The authors are thankful to the Austrian Science Fund (FWF) for the financial support within projects P20902-N10 and P23143-N21. Coauthor David Salstein is sponsored in part by grant ATM-091370 from the U.S. National Science Foundation (NSF). The use of meteorological data of the ECMWF and NASA's GMAO is greatly appreciated, and we also thank O. de Viron as well as another (anonymous) reviewer for their valuable comments and suggestions.

References

Barnes, R., R. Hide, A. White, and C. Wilson (1983), Atmospheric angular momentum fluctuations, length-of-day changes and polar motion, *Proc. R. Soc. Lond.*, *A387*, 31–73.

Bell, M. J. (1994), Oscillations in the equatorial components of the atmosphere's angular momentum and torques on the earth's bulge, *Q. J. R. Meteorol. Soc.*, *120*, 195–213.

Bosch, K. (1996), *Großes Lehrbuch der Statistik*, Oldenbourg, München. ISBN: 3-486-23350-5.

Brzeziński, A. (1994), Polar motion excitation by variations of the effective angular momentum function, II: Extended-model, *Manuscr. Geodetica*, *19*, 157–171.

Brzeziński, A., J. Nastula, and B. Kolaczek (2009), Seasonal excitation of polar motion estimated from recent geophysical models and observations, *J. Geodyn.*, *48*, 235–240, doi:10.1016/j.jog.2009.09.21.

Chen, J. L., C. R. Wilson, B. F. Chao, C. K. Shum, and B. D. Tapley (2000), Hydrological and oceanic excitations to polar motion and length-of-day variations, *Geophys. J. Int.*, *141*, 149–156, doi:10.1046/j.1365-246X.2000.00069.x.

Dee, D. P., et al. (2011), The ERA-Interim reanalysis: Configuration and performance of the data assimilation system, *Q. J. R. Meteorol. Soc.*, *137*, 553–597, doi:10.1002/qj.828.

de Viron, O., and V. Dehant (2003), Tests on the validity of atmospheric torques on Earth computed from atmospheric model outputs, *J. Geophys. Res.*, *108*, B22068, doi:10.1029/2001JB001196.

de Viron, O., C. Bizouard, D. Salstein, and V. Dehant (1999), Atmospheric torque on the Earth and comparison with atmospheric angular momentum variations, *J. Geophys. Res.*, *104*(B3), 4861–4875, doi:10.1029/1999JB900063.

de Viron, O., R. M. Ponte, and V. Dehant (2001), Indirect effect of the atmosphere through the oceans on the Earth nutation using the torque approach, *J. Geophys. Res.*, *106*(B5), 8841–8851.

de Viron, O., L. Koot, and V. Dehant (2005a), Polar motion models: The torque approach, in *Forcing of Polar motion in the Chandler Frequency Band: A Contribution to Understanding Interannual Climate Change, Luxembourg, 21–23 April, 2004, Cahiers du Centre Européen de Géodynamique et du Séismologie,* vol. 24, edited by H. P. Plag et al., pp. 9–14, European Seismological Commission, Luxembourg.

de Viron, O., G. Schwarzbaum, F. Lott, and V. Dehant (2005b), Diurnal and subdiurnal effects of the atmosphere on the Earth rotation and geocenter motion, *J. Geophys. Res.*, *110*, B11404, doi:10.1029/2005JB003761.

Dill, R., (2009), Hydrological model LSDM for operational Earth rotation and gravity field variations, *Sci. Tech. Rep., 08/09*, Deutsches GeoForschungsZentrum, Potsdam, Germany.

Dobslaw, H., R. Dill, A. Grötzsch, A. Brzeziński, and M. Thomas (2010), Seasonal polar motion excitation from numerical models of atmosphere, ocean and continental hydrosphere, *J. Geophys. Res.*, *115*, B10406, doi:10.1029/2009JB007127.

Eubanks, T. M., J. A. Steppe, J. O. Dickey, R. D. Rosen, and D. A. Salstein (1988), Causes of rapid motions of the Earth's pole, *Nature*, *334*, 115–119.

Feldstein, S. B. (2008), The dynamics of atmospherically driven intraseasonal polar motion, *J. Atmos. Sci*, *65*, 2290–2307, doi:10.1175/2007JAS2640.1.

Fujita, M., B. F. Chao, B. V. Sanchez, and T. J. Johnson (2002), Oceanic torques on solid Earth and their effects on Earth rotation, *J. Geophys. Res.*, *107*(B7), 2154, doi:10.1029/2001JB000339.

Greiner-Mai, H., and F. Barthelmes (2001), Relative wobble of the Earth's inner core derived from polar motion and associated gravity variations, *Geophys. J. Int.*, *144*(1), 27–36.

Gross, R. S. (2007), Earth rotation variations – long period, in *Physical Geodesy,* vol. 3, edited by T. A. Herring, pp. 239–294, Treatise on Geophysics, Elsevier, Oxford.

Gross, R. S., I. Fukumori, and D. Menemenlis (2003), Atmospheric and oceanic excitation of the Earth's wobbles during 1980–2000, *J. Geophys. Res.*, *108*(B8), 2370, doi:10.1029/2002JB002143.

Huang, H. P., and K. M. Weickmann (2008), On the computation of the mountain torque from gridded global datasets, *Mon. Weather Rev.*, *136*, 4005–4009, doi:10.1175/2008MWR2359.1.

Huang, H., P. D. Sardeshmukh, and K. M. Weickmann (1999), The balance of global angular momentum in a long-term atmospheric data set, *J. Geophys. Res.*, *104*(D2), 2031–2040.

Jenkins, G. M., and D. G. Watts (1968), *Spectral Analysis and its Applications*, Holden-Day, San Francisco.

Kalnay, E., et al. (1996), The NCEP/NCAR 40-year reanalysis project, *Bull. Amer. Meteor. Soc.*, *77*(3), 437–471.

Kursinski, E. R., G. A. Hajj, R. Schofield, P. Linfield, and K. R. Hardy (1997), Observing Earth's atmosphere with radio occultation measurements using the Global Positioning System, *J. Geophys. Res.*, *102*(D19), 23,429–23,465, doi:10.1029/97JD01569.

Lott, F., O. de Viron, P. Viterbo, and F. Vial (2008), Axial atmospheric angular momentum budget at diurnal and subdiurnal periodicities, *J. Atmos. Sci.*, *65*, 156–171, doi:10.1175/2007JAS2178.1.

Marcus, S. L., O. de Viron, and J. O. Dickey (2004), Atmospheric contributions to Earth nutation: Geodetic constraints and limitations of the torque approach, *J. Atmos. Sci.*, *61*, 352–356.

Marcus, S. L., O. de Viron, and J. O. Dickey (2010), Interannual atmospheric torque and El-Niño-Southern Oscillation: Where is the polar motion signal? *J. Geophys. Res.*, *115*, B12409, doi:10.1029/2010JB007524.

Masaki, Y. (2008), Wind field differences between three meteorological reanalysis data sets detected by evaluating atmospheric excitation of Earth rotation, *J. Geophys. Res.*, *113*, D07110, doi:10.1029/2007JD008893.

Moritz, H., and I. I. Müller (1987), *Earth Rotation: Theory and Observation*, Ungar, New York.

Munk, W., and G. Groves (1952), The effect of winds and ocean currents on the annual variation in latitude, *J. Meteorol.*, *9*(6), 385–396.

Munk, W. H., and G. J. F. MacDonald (1960), *The Rotation of the Earth: A Geophysical Discussion*, Cambridge University Press, New York.

Nastula, J., and D. Salstein (1999), Regional atmospheric angular momentum contributions to polar motion excitation, *J. Geophys. Res.*, *104*(B4), 7347–7358, doi:10.1029/1998JB900077.

Ponte, R. M. (1997), Oceanic excitation of daily to seasonal signals in Earth rotation: Results from a constant-density numerical model, *Geophys. J. Int.*, *130*(2), 469–474.

Ponte, R. M., D. Stammer, and J. Marshall (1998), Oceanic signals in observed motions of the Earth's pole of rotation, *Nature*, *391*, 476–479, doi:10.1038/35126.

Proakis, J. G., and D. G. Manolakis (1996), *Digital Signal Processing: Principles, Algorithms, and Applications*, 3rd edition, Prentice Hall, New Jersey.

Rienecker, M. M., et al. (2011), MERRA: NASA's modern-era retrospective analysis for research and applications, *J. Climate*, *24*, 3624–3648.

Rosen, R. D., and D. A. Salstein (1983), Variations in atmospheric angular momentum on global and regional scales and the length of day, *J. Geophys. Res.*, *88*(C9), 5451–5470.

Saha, S., et al. (2010), The NCEP climate forecast system reanalyis, *Bull. Amer. Meteor. Soc.*, *91*, 1015–1057.

Salstein, D. A., and R. D. Rosen (1994), Topographic forcing of the atmosphere and a rapid change in the length of day, *Science*, *264*(5157), 405–409.

Schindelegger, M., J. Böhm, D. Salstein, and H. Schuh (2011), High-resolution atmospheric angular momentum functions related to Earth rotation parameters during CONT08, *J. Geod.*, *7*, 425–433, doi:10.1007/s00190-011-0458-y.

Schindelegger, M., J. Böhm, and D. Salstein (2013), Seasonal and intraseasonal polar motion variability as deduced from atmospheric torques, *J. Geod. Geoinf.*, *1*, 89–95, doi:10.9733/jgg.231112.1.

Swinbank, R. (1985), The global atmospheric angular momentum balance inferred from analyses made during FGGE, *Quart. J. R. Met. Soc.*, *111*, 977–992.

Thomas, M., J. Sündermann, and E. Maier-Reimer (2001), Consideration of ocean tides in an OGCM and impacts on subseasonal to decadal polar motion excitation, *Geophys. Res. Lett.*, *28*(12), 2457–2460.

Wahr, J. M. (1982), The effects of the atmosphere and the oceans on the Earth's wobble – I. Theory, *Geophys. J. R. Astron. Soc.*, *70*, 349–372.

Wahr, J. M. (1983), The effects of the atmosphere and the oceans on the Earth's wobble and on the seasonal variations in the length of day – II. Results, *J. R. Astron. Soc.*, *74*, 451–487.

White, R. M. (1949), The role of the mountains in the angular-momentum balance of the atmosphere, *J. Atmos. Sci.*, *6*(5), 353–355.